A&A 520, A48 (2010)
DOI: 10.1051/0004-6361/201014834
© ESO 2010

Astronomy & Astrophysics

A VLT/FLAMES survey for massive binaries in Westerlund 1

II. Dynamical constraints on magnetar progenitor masses from the eclipsing binary W13⋆

B. W. Ritchie[1,2], J. S. Clark[1], I. Negueruela[3], and N. Langer[4,5]

[1] Department of Physics and Astronomy, The Open University, Walton Hall, Milton Keynes MK7 6AA, UK
e-mail: b.ritchie@open.ac.uk
[2] IBM United Kingdom Laboratories, Hursley Park, Winchester, Hampshire SO21 2JN, UK
[3] Departamento de Física, Ingeniería de Sistemas y Teoría de la Señal, Universidad de Alicante, Apdo. 99, 03080 Alicante, Spain
[4] Argelander-Institut für Astronomie der Universität Bonn, Auf dem Hügel 71, 53121 Bonn, Germany
[5] Astronomical Institute, Utrecht University, Princetonplein 5, Utrecht, The Netherlands

Received 21 April 2010 / Accepted 14 June 2010

ABSTRACT

Context. Westerlund 1 is a young, massive Galactic starburst cluster that contains a rich coeval population of Wolf-Rayet stars, hot- and cool-phase transitional supergiants, and a magnetar.
Aims. We use spectroscopic and photometric observations of the eclipsing double-lined binary W13 to derive dynamical masses for the two components, in order to determine limits for the progenitor masses of the magnetar CXOU J164710.2-455216 and the population of evolved stars in Wd1.
Methods. We use eleven epochs of high-resolution VLT/FLAMES spectroscopy to construct a radial velocity curve for W13. *R*-band photometry is used to constrain the inclination of the system.
Results. W13 has an orbital period of 9.2709 ± 0.0015 days and near-contact configuration. The shallow photometric eclipse rules out an inclination greater than 65°, leading to lower limits for the masses of the emission-line optical primary and supergiant optical secondary of 21.4 ± 2.6 $M_\odot$ and 32.8 ± 4.0 $M_\odot$ respectively, rising to $23.2^{+3.3}_{-3.0}$ $M_\odot$ and $35.4^{+5.0}_{-4.6}$ $M_\odot$ for our best-fit inclination 62^{+3}_{-4} degrees. Comparison with theoretical models of Wolf-Rayet binary evolution suggest the emission-line object had an initial mass in excess of ∼35 $M_\odot$, with the most likely model featuring highly non-conservative late-Case A/Case B mass transfer and an initial mass in excess of 40 $M_\odot$.
Conclusions. This result confirms the high progenitor mass of the magnetar CXOU J164710.2-455216 inferred from its membership in Wd1, and represents the first dynamical constraint on the progenitor mass of any magnetar. The red supergiants in Wd1 must have similar progenitor masses to W13 and are therefore amongst the most massive stars to undergo a red supergiant phase, representing a challenge for population models that suggest stars in this mass range end their redwards evolution as yellow hypergiants.

Key words. stars: evolution – supergiants – stars: individual: W13 – stars: magnetars – binaries: general

1. Introduction

The Galactic starburst cluster Westerlund 1 (hereafter Wd1; Westerlund 1961; Clark et al. 2005) contains a rich coeval population of OB supergiants, yellow hypergiants (YHGs) and red supergiants (RSGs) that collectively map out the transitional post-Main Sequence (MS) loop redwards followed by massive stars in the cluster. The relative brevity of the transitional phase and intrinsic rarity of such objects means that this stage of evolution is poorly understood, but recent downward revisions to MS mass loss rates (Fullerton at al. 2006; Mokiem et al. 2007) suggest that it is of critical importance in understanding how massive stars shed their outer layers prior to the Wolf-Rayet (WR) phase.

Due to its unique stellar population, Wd1 has been the subject of intensive observational study in recent years (Ritchie et al. 2009a, hereafter Paper I, and refs. therein; see also Clark et al. 2010a; Negueruela et al. 2010). Studies of the massive stellar population support a single burst of star formation at an age ∼5 Myr and a distance ∼5 kpc (Crowther et al. 2006; Negueruela et al. 2010), with the identification of ∼O8V stars in the cluster (Clark et al., in prep.) and a population of lower-luminosity late-O II−III stars just evolving off the MS both fully consistent with this derived age. Dynamical mass determinations of late-O dwarfs (Gies 2003) and comparison of the population of OB stars in Wd1 with theoretical isochrones (Meynet & Maeder 2000) suggest that stars with $M_{\rm ini} \sim 30\ M_\odot$ lie at the MS turn-off, with the early-B supergiants having progenitor masses $M_{\rm ini} \sim 35{-}40\ M_\odot$ (Negueruela et al. 2010) and the WR population descended from stars with $M_{\rm ini} \geq 40\ M_\odot$ (Crowther et al. 2006). However, to date no direct mass determination exists for a member of Wd1; as well as providing confirmation of the current understanding of the cluster derived from spectroscopic studies, this is of importance for confirming the high progenitor mass for the magnetar CXOU J164710.2-455216 that has been inferred from its membership of Wd1 (Muno et al. 2006). In addition, the distribution of evolved stars in Wd1 offers the prospect of demanding tests for evolutionary models, with both the distribution

⋆ This work is based on observations collected at the European Southern Observatory under programme IDs ESO 81.D-0324 and 383.D-0633.

of WR subtypes and the large number of cool hypergiants in both YHG and RSG phases at odds with current predictions (Clark et al. 2010a).

In this paper we present spectroscopic radial velocity (RV) measurements of the massive binary W13, identified as a 9.2-day eclipsing system by Bonanos (2007). X-ray observations reveal a hard source with $L_X \sim 10^{32}$ erg s^{-1}, consistent with a colliding-wind system (Clark et al. 2008), while subsequent multi-epoch spectroscopy described in Paper I showed W13 to be a double-lined spectroscopic binary consisting of a B0.5Ia$^+$/WNVL emission-line object[1] and an early-B supergiant. We supplement the results of Paper I with an additional six epochs of data, providing a total baseline of approximately 14 months that allows an accurate radial velocity curve to be derived for the W13 system. This is used in conjunction with *R*-band photometry (Bonanos 2007) to determine the masses of the two components.

2. Observations and data reduction

Spectra of W13 were obtained on eight epochs in 2008 and three epochs in 2009 using the Fibre Large Array Multi Element Spectrograph (FLAMES; Pasquini et al. 2002), located on VLT UT2 *Kueyen* at Cerro Paranal, Chile. The GIRAFFE spectrograph was used in MEDUSA mode with setup HR21 to cover the 8484−9001 Å range with resolution $R \sim 16\,200$; full details of data acquisition and reduction are given in Paper I, and representative spectra showing the Pa11 λ8862 and Pa12 λ8750 lines at two extremes of the RV curve are shown in Fig. 1. The signal-to-noise (S/N) ratio of our spectra is ∼95 at 8700 Å. Photometry of W13 was taken from the published data of Bonanos (2007), obtained on 17 nights between 15/6/2006 and 25/7/2006 using the 1m Swope telescope at Las Campanas Observatory, Chile.

RV measurements were carried out using the IRAF[2] *onedspec* tasks to fit Gaussian profiles to the cores of the Paschen series absorption and emission features in the spectrum of W13: the derived RV at each epoch is an error-weighted average of the RV of individual lines. Strong interstellar C_2 lines from the (2, 0) Phillips band overlap the Pa12 line, leading to a systematic phase-dependent bias of up to ∼10 km s^{-1} in the line centre, and this line was therefore excluded from the analysis. In addition, a broad DIB centred at ∼8648 Å (Negueruela et al. 2010) overlaps the Pa13 λ8665 line, attenuating the blue flank of the emission component at $\phi \sim 0.25$ and leading to an offset redwards relative to the other Paschen series lines, although measurement of the absorption component is not affected. Finally, at $\phi \sim 0.15$−0.3 a systematic decrease in strength is seen in all Paschen-series emission lines, with the lines recovering in strength rapidly after $\phi \sim 0.3$; this can be seen in the right panel of Fig. 1, which overplots five spectra taken at $\phi \sim 0.15$−0.35. The weakening in Paschen-series emission was assumed to be wind variability in Paper I, but the persistence of this behaviour over more than ∼30 orbits in our extended dataset implies that it is not a transitory effect but rather a region of excess absorption periodically crossing the line of sight.

[1] The WNVL classification is used here to indicate strong spectroscopic similarities with other WNL stars in Wd1; we note the He II λ4686 line necessary for formal classification (Crowther & Smith 1996) lies outside our spectral coverage.

[2] IRAF is distributed by the National Optical Astronomy Observatories, which are operated by the Association of Universities for Research in Astronomy, Inc., under cooperative agreement with the National Science Foundation.

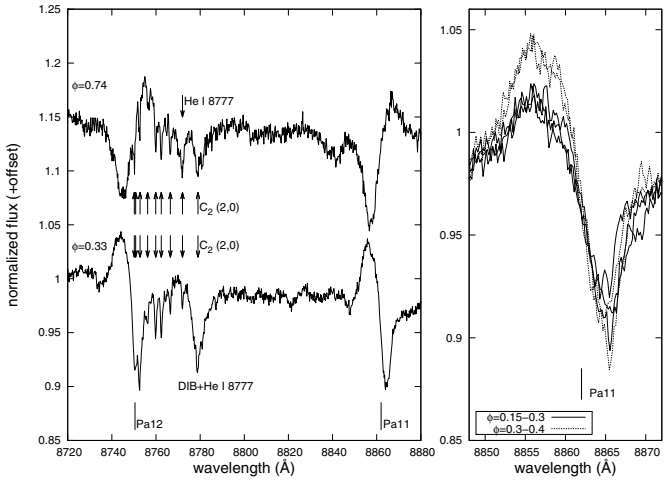

Fig. 1. *Left panel*: *I*-band spectra of W13 at $\phi = 0.33$ and $\phi = 0.74$. *Right Panel*: phase dependent variability of the Pa12 emission line. Five spectra are overplotted, with three from $\phi = 0.15$−0.30 (solid line) and two from $\phi = 0.30$−0.35 (dotted line).

Absorption line RV measurements were therefore carried using the Pa11 and Pa13−16 lines, noting that the weakening of the higher Paschen-series lines leads to an increased fitting error and consequent decreased weight in the derived RV. Emission line RV measurements were carried out as follows:

- Emission lines cannot be measured with accuracy for one spectrum taken near eclipse ($\phi = 0.03$, 24/07/2008, MJD = 54 671.13).
- At $\phi = 0.1$–0.3 attenuation of the blue flank of Pa13 by the ∼8648 Å DIB and the decrease in strength of Pa15 and Pa16 leave only Pa11 and Pa14 emission lines available for measurement, with the two lines in good agreement.
- At other epochs, Pa11 and Pa13–16 emission components were measured.

3. Results

3.1. Spectroscopic classification

3.1.1. The optical primary

The *R*-band spectrum of W13 is dominated by the emission-line optical primary, with strong, relatively broad Hα emission (*FWHM* ∼ 500 km s^{-1}), complex, time-varying P Cygni profiles extending to at least −350 km s^{-1} in the He I $\lambda\lambda$6678, 7065 lines and weak C II $\lambda\lambda$6578, 6582 emission. A comparison of previously published intermediate-resolution *R*-band spectra of W13 and the blue hypergiants W5/WR S (B0.5Ia$^+$/WN10−11; Negueruela & Clark 2005) and W7 (B5Ia$^+$; Negueruela et al. 2010) is shown in Fig. 2. The luminous mid-late B hypergiants in Wd1[3] are all believed to be on a pre-RSG loop redwards (Clark et al. 2010b), and display narrow Hα profiles with strong P Cygni absorption components, along with He I and C II in absorption (Clark et al. 2010a; Negueruela et al. 2010). In contrast, the spectrum of W13 shows strong similarities to both W5 and the WN9h binary W44/WR L (Crowther et al. 2006; Clark et al. 2010a), with the three objects forming a morphologically-distinct group when compared to the mid-late B hypergiants,

[3] W7, W33, and W42a; B5–B9Ia$^+$ (Negueruela et al. 2010).

Table 1. Journal of observations.

Date	MJD[a]	Phase[b]	Elapsed orbits[b]	RV_{abs} (km s^{-1})	RV_{em} (km s^{-1})
29/06/2008	54 646.1846	0.33	0.33	+54 ± 9	−232 ± 7
18/07/2008	54 665.0356	0.37	2.37	+39 ± 8	−246 ± 18
24/07/2008	54 671.1343	0.03	3.03	−50 ± 11	–
14/08/2008	54 692.0423	0.28	5.28	+74 ± 13	−224 ± 14
04/09/2008	54 713.0107	0.55	7.55	−120 ± 5	+127 ± 29[c]
15/09/2008	54 724.0818	0.74	8.74	−200 ± 9	+163 ± 11
19/09/2008	54 728.0554	0.17	9.17	+56 ± 4	−225 ± 17
25/09/2008	54 734.0613	0.82	9.82	−173 ± 7	+164 ± 9
14/05/2009	54 965.1768	0.76	34.76	−214 ± 14	+137 ± 8
18/05/2009	54 969.3198	0.21	35.21	+76 ± 13	−242 ± 7
20/08/2009	55 063.0575	0.32	45.32	+78 ± 11	−217 ± 16

Notes. [(a)] Modified Julian day at the midpoint of two 600 s integrations (2 × 500 s, 04/09/2008; 1 × 600 s + 1 × 700 s, 19/09/2008). [(b)] Phase taking T_0 = 54 643.080, elapsed orbits for an orbital period of 9.271d (see Sect. 3.2). [(c)] Unreliable due to the appearance of a central reversal in the emission line, and excluded from the fit to the RV curve.

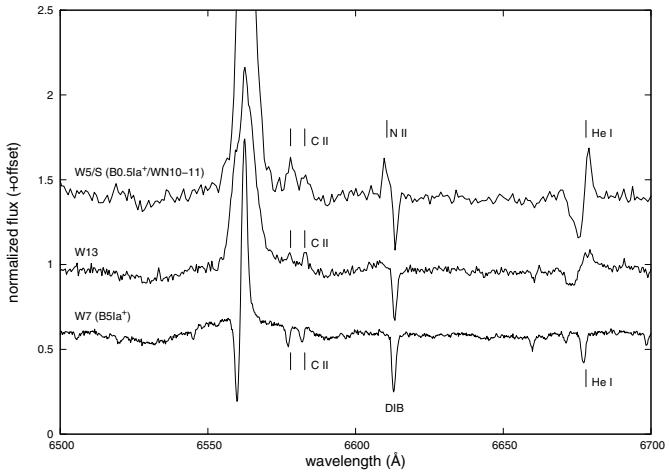

Fig. 2. Intermediate-resolution spectra of W13 and the blue hypergiants W5 (B0.5Ia$^+$/WN10–11, top) and W7 (B5Ia$^+$, bottom). Spectra taken from Clark et al. (2010a) and Negueruela et al. (2010).

suggesting that the emission-line object in W13 is also an immediate evolutionary precursor to the WR phase.

The spectrum plotted in Fig. 2 shows He I lines that are redshifted by ∼50 km s^{-1} and C II emission lines somewhat bluewards of He I (RV ∼ 0 km s^{-1}), although accurate measurement of the C II line centres is difficult due to their low strength and the relatively low S/N of the R-band spectrum. Nevertheless, if the C II lines originated in the companion then we would expect the lines to be significantly blueshifted at this epoch (RV ∼ −150 km s^{-1}; see Sect. 3.2), suggesting that the emission lines have a common origin[4]. However, N II λ6611 emission, present in both W5 and W44, appears absent in W13, while the Hα, He I and C II emission lines are also considerably weaker, suggesting W13 is the least evolved member of the WNVL population of Wd1.

3.1.2. The optical secondary

The Paschen-series lines display complex emission/absorption profiles with the two components moving in anti-phase (see Fig. 1). The absorption components have similar strengths to the lower-luminosity O9.5Iab/b objects in our FLAMES dataset, but infilling from the emission-line object is likely to affect these features and an alternative diagnostic is provided by weak He I λ8584, 8777 absorption lines that are apparent in many spectra, moving in phase with the Paschen-series absorption lines. These He I lines are first seen at O8−9I and strengthen rapidly at ∼B1.5I (Negueruela et al. 2010), with their weakness therefore suggesting a spectral type no later than ∼B1I, although overlapping interstellar features (including a broad, weak DIB at ∼8779 Å) preclude precise measurement. A late-O spectral type appears to be excluded by the apparent absence of C III λ8500 absorption, with this line leading to a bluewards offset and discrepant strength for the C III λ8500/Pa16 λ8502 blend in the O9.5−B0.5 supergiants in Wd1 (Negueruela et al. 2010; see also Paper I). Neither classifier should be significantly affected by wind emission[5], and the weak He I lines and absence of C III absorption therefore suggests a ∼B0.5−1I classification with an uncertainty of roughly half a spectral subtype and lack of strong constraints on the luminosity class. However, we caution that if C III is weak due to abundance anomalies or near-critical rotation then this limit may not apply, and the weakness of the He I lines permit a classification of O9.5−B0I that is broadly consistent with the Paschen-series line strengths.

3.2. Radial velocity curve

Figure 3 shows RV curves for the two components of the W13 system. Taking the 9.20-day period reported by Bonanos (2007) as a starting point, an error-weighted χ^2 fit to the radial velocities of the absorption-line component yielded best-fit values for the orbital period of P = 9.2709 ± 0.0015 days, consistent with an independent determination using a Lomb-Scargle periodogram (Press & Rybicki 1989), a systemic velocity of −65.9 ± 2.4 km s^{-1} and semi-amplitude K_{abs} = 137.3 ± 6.7 km s^{-1}. The corresponding fit to the emission line RV curve[6] has a systemic velocity of −48.2 ± 3.1 km s^{-1} and semi-amplitude K_{em} = 210.2 ± 8.7 km s^{-1}. Errors are derived from the fitting residuals using the bootstrap method (Efron & Tibshirani 1994). We note that systemic velocity derived from the emission

[4] We note that W5 also appears to show C II blueshifted relative to He I.

[5] The He I λ8584, 8777 lines arise from transitions from the 3p^{3}P° level, which is well-populated in ∼B1−4 supergiants, to upper levels near the ionisation limit of He I (van Helden 1972), but the corresponding downwards transitions are very weak.

[6] In fitting the emission-line RV curve, the discrepant point at ϕ = 0.55 was excluded.

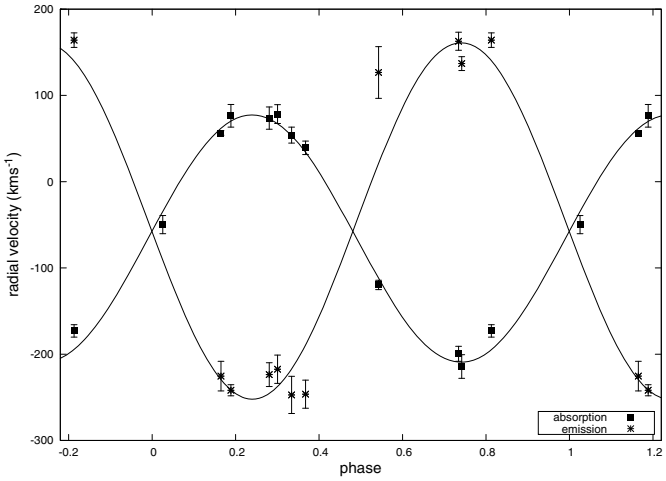

Fig. 3. Radial velocity curve for W13.

line fit is somewhat lower than that derived from the companion, and is in closer agreement with the mean radial velocities of other Wd1 supergiants (see Paper I). Discrepancies in this parameter are commonly observed in early-type spectroscopic binaries (e.g. the 9.8-day O7III(f)+O8.5I binary HD 149404; Rauw et al. 2001) although the effect is small in comparison with some other evolved systems (e.g. HDE 228766; Massey & Conti 1977; Rauw et al. 2002) in which wind contamination strongly affects derived systemic velocities.

Taking these values yields a mass ratio $q = M_{\rm abs}/M_{\rm em} = 1.53 \pm 0.10$ and masses for the two components of:

$$M_{\rm em} \sin^3 i = \frac{(1+q)^2 P K_{\rm abs}^3}{2\pi G} = 15.9 \pm 1.9\ M_\odot \quad (1)$$

and

$$M_{\rm abs} \sin^3 i = 24.4 \pm 3.0\ M_\odot \quad (2)$$

Finally, measurements of blended hydrogen lines with Gaussian fits tend to yield systematically lower values of K_1 and K_2 than methods such as spectral disentangling (Simon & Sturm 1994) that are less affected by blending (Andersen 1975; Southworth & Clausen 2007). The paucity of strong lines free from significant interstellar, telluric and wind contamination in the *R*- and *I*-band spectra of ~B0 supergiants makes the extent of this effect on our determination of $K_{\rm em}$ and $K_{\rm abs}$ hard to quantify, and we therefore note that our method may underestimate the masses of the two components of W13.

3.3. Light curve

To constrain $\sin^3 i$, we folded the *R*-band photometric data reported by Bonanos (2007) on to the 9.271 day period determined from the RV data. The data were binned to reduce the considerable scatter present in the light curve, which is most probably a consequence of intrinsic aperiodic variability in one or both components: low-level photometric and spectroscopic variability is a feature of all transitional supergiants in Wd1, with the blue hypergiants displaying rapid photometric variability at the ~0.1 mag level and the early-B supergiants also variable (Bonanos 2007; Clark et al. 2010a). Therefore, given the limited dataset and shallow ~0.15 mag eclipse, we do not expect to be able to fit the light curve of W13 with high accuracy.

Table 2. Summary of orbital and physical parameters of W13[a].

Parameter	Value	
T_0 (MJD)[a]	54 643.080	
P (days)	9.2709 ± 0.0015	
$q = m_{\rm abs}/m_{\rm em}$	1.53 ± 0.10	
a ($R_\odot$)	72±3	
e	0 (fixed)	
i	$62^{+3\,\circ}_{-4}$	
	Emission	Absorption
Filling factor	0.93 ± 0.05	0.74 ± 0.1
$T_{\rm eff}$ (K)	25 000 (fixed)	25 000 ± 2000
R ($R_\odot$)	22 ± 2	21 ± 2
γ (km s^{-1})	−48.2 ± 3.1	−65.9 ± 2.4
K (km s^{-1})	210.2 ± 8.7	137.3 ± 6.7
$M\sin^3 i$ ($M_\odot$)	15.9 ± 1.9	24.4 ± 3.0
$M(i = 65^\circ)$ ($M_\odot$)	21.4 ± 2.6	32.8 ± 4.0
$M(i = 62^{+3\circ}_{-4})$ ($M_\odot$)	$23.2^{+3.3}_{-3.0}$	$35.4^{+5.0}_{-4.6}$

Notes. [(a)] Note that T_0 corresponds to the eclipse of the B0.5Ia$^+$ emission-line star.

Nevertheless, in the absence of longer-term photometric monitoring, the data of Bonanos (2007) allow reasonable constraints to be placed on the orbital inclination.

The *nightfall* code[7] was used to model the light curve of W13. The effective temperature of the emission line object was fixed at 25 kK, appropriate for its spectral type, and a linear limb-darkening law and circular orbits were assumed. The mass ratio was derived from the RV curve, and the inclination, Roche lobe filling factors for both objects and temperature of the optical secondary were allowed to vary. The code rapidly converges to a near-contact configuration in which the emission-line object has almost filled its Roche lobe (filling factor ~0.93 ± 0.05) and the other star has a somewhat lower filling factor (~0.74 ± 0.1). The best-fit model has an inclination $i = 62^\circ$ and provides a close match to the light curve from $\phi \sim 0.5$ to $\phi \sim 1$, although the region around $\phi = 0.2$–0.4 is less well reproduced. Although the *nightfall* code supports additional features such as "hot spots" that may provide a better fit to this portion of the light curve (see, for example, the model of Cyg OB2#5 presented by Linder et al. 2009), we consider further refinement of the model inappropriate given the limitations of the photometric dataset used. Parameters derived from the light curve model are listed in Table 2, although we stress that our primary goal is to constrain the inclination of the system and other parameters should be regarded as provisional pending acquisition of longer-term photometry.

To examine errors in the derived inclination we investigated models in which i is fixed at values from 55° to 68° while filling factors and temperatures are allowed to vary as before; the best fit $i = 62^\circ$ curve and models with $i = 59^\circ$, $i = 65^\circ$ and $i = 68^\circ$ are plotted in Fig. 4. Inclinations greater than our best-fit model lead to slightly lower filling factors and higher temperatures, while the converse is true for lower inclinations. The depth of the eclipse provides the strongest constraint on the model, with inclinations greater than ~65° strongly disfavoured. *I*-band photometry is also presented by Bonanos (2007), but considerably greater scatter is present in the data at mid-eclipse, making it less suitable for modelling. Nevertheless, these data also support $i \leq 65^\circ$, favouring a value ~60–62°, although the degree of scatter renders this uncertain. Therefore, taking $i \leq 65^\circ$ places robust lower

[7] http://www.hs.uni-hamburg.de/DE/Ins/Per/Wichmann/Nightfall

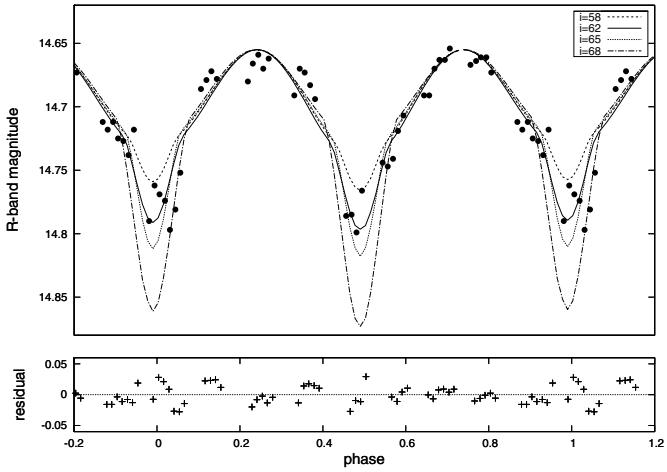

Fig. 4. Fit to the *R*-band lightcurve of W13.

limits of $M_{\rm em} \geq 21.4 \pm 2.6\ M_\odot$ and $M_{\rm abs} \geq 32.8 \pm 4.0\ M_\odot$ for the emission-line object and its companion, rising to $23.2^{+3.3}_{-3.0}\ M_\odot$ and $35.4^{+5.0}_{-4.6}\ M_\odot$ for our preferred inclination $i = 62^{+3}_{-4}{}^\circ$. For the purposes of discussion we take the lower masses derived from the $i \leq 65^\circ$ limit.

4. Discussion and conclusions

4.1. The evolution of the W13 system

The short orbital period, near-contact configuration and evolved, mass-depleted nature of the emission-line object all imply that the two components of the W13 system must have undergone strong interaction during their evolution. The 9.3-day orbital period suggests a late-Case A or Case B scenario, with mass transfer beginning near the onset of shell hydrogen burning (Petrovic et al. 2005, hereafter P05). The presence of unevolved late-O stars ($M_{\rm ini} \sim 30\ M_\odot$) in Wd1 suggests a minimum initial mass $\sim$35 $M_\odot$ for shell burning to have commenced, with in excess of $\sim$10 $M_\odot$ lost once mass transfer begins. However, transfer of angular momentum is expected to lead to the accretor rapidly reaching critical rotation (Packet 1981; Langer et al. 2008), while rapid rotation will also greatly increase wind mass loss rates (Langer 1998), and a fully-conservative transfer scenario appears unlikely. Indeed, models of short-period WR+O binaries by P05 suggests that mass-transfer is highly *non*-conservative in such scenarios, with only $\sim$10% of transferred mass being retained by companion star. The current 21 $M_\odot$ + 33 $M_\odot$ (minimum) mass ratio in W13 is consistent with the P05 model of late-Case A/Case B evolution at low accretion efficiency, with higher accretion efficiencies leading to a more unequal mass ratio than we observe.

P05 estimate a relationship between initial MS mass and final WR mass for Case B systems of $M_{\rm ini} = (M_{\rm WR} + 4.2)/0.53$ that suggests that the emission-line object had an initial mass $\sim$48 $M_\odot$. While this is consistent with estimates of WR progenitor masses (Crowther et al. 2006), it is somewhat higher than expected for a star just entering the WR phase in Wd1. However, W13 will likely shed further mass before becoming a *bona fide* WN9, suggesting that $M_{\rm WR} \sim 20\ M_\odot$ and consequent initial MS mass around $\sim$45 $M_\odot$ are more appropriate. Assuming an accretion efficiency of $\sim$10% from P05, this would imply that $\sim$2–3 $M_\odot$ was transferred to the secondary, with the remainder lost from the system. While extended radio emission from W13 is not detected (Dougherty et al. 2010), emission from both the O9Ib star W15 and the extreme RSG W26 overlaps the region around W13 and might obscure direct signs of recent mass loss.

W13 therefore appears to be a less-evolved analogue to WR21 (HD 90657), a 8.3-day 19 + 37 $M_\odot$ WN5 binary considered by P05. One notable discrepancy is the presence of an evolved companion in W13, whereas WR21 contains an unevolved mid-O star. Although abundance anomalies might suppress the C III λ8500 line in a late-O supergiant, leading to an erroneously late spectral type, the presence of He I lines moving in phase with the Paschen-series absorption lines excludes a spectral type earlier than $\sim$O9 (Negueruela et al. 2010). It is possible that the supergiant is still in extreme, near-critical rotation from recent mass transfer, and is thus expanded with a complex, latitude-dependent spectrum that features both hot (polar) and cooler (equatorial) components. However, confirmation of this hypothesis is observationally challenging, as infilling of the Paschen-series absorption lines prevents direct determination of v sin$i$ while the high reddening towards Wd1 precludes the use of fiducial O-type spectral classifiers in the blue region of the spectrum.

4.2. Evolutionary implications for Wd1

4.2.1. The cool hypergiant population of Wd1

The likely $\geq$40 $M_\odot$ MS mass for the emission-line object in W13 provides direct constraints on the masses of the eleven cool hypergiants in Wd1. Of these, only two have been studied in detail[8], but the long-term dataset compiled by Clark et al. (2010a) reveal a remarkable *lack* of secular evolution amongst these objects, with only the LBV W243 (Ritchie et al. 2009b) apparently undergoing a major outburst in the half-century since the discovery of the cluster by Westerlund (1961). Although early observations are sparse, the available data are sensitive to the long-term evolutionary trends seen in objects such as the YHG IRC +10 420 (Humphreys et al. 2002), the LBV R127 (Walborn et al. 2008) or M 33's Var A (Humphreys et al. 2006). Current observations therefore suggest the supergiants in Wd1 undergo a slow redwards evolution at approximately constant luminosity until they encounter an extended cool-phase state accompanied by growing pulsational instability (Clark et al. 2010a,b).

Evolutionary models of massive stars predict a relatively long YHG lifetime at $T \sim 6000$ K for stars with $M_{\rm ini} \sim 40\ M_\odot$, consistent with the lack of secular evolution and mid-A to late-F spectral types for the YHGs in Wd1, but do not predict further evolution to the RSG phase (Meynet & Maeder 2003; Drout et al. 2009). However, while the B- and A/F-hypergiant populations plotted in Fig. 5 appear in good agreement with the evolutionary tracks[9], the presence of RSGs in Wd1 suggests that stars in this mass range *do* evolve further redwards (Clark et al. 2010a), with the extended radio nebulae around these objects (Dougherty et al. 2010) revealing extensive mass loss that may account for a significant fraction of the mass lost prior to the WR phase. Lower-mass stars will not reach the RSG phase until $\geq$6 Myr, and the absence of any other indicators of significant

[8] The A3Ia$^+$ LBV W243 (Ritchie et al. 2009b) and the YHG W265, which varies from F1–5Ia$^+$ with a $\sim$100 day quasi-period (Paper I; also Clark et al. 2010a).

[9] Luminosities for the BHGs W7 and W33 are taken from Negueruela et al. (2010), while the luminosity of the LBV W243 is taken from non-LTE modelling assuming a distance of 5 kpc (Ritchie et al. 2009b). YHG luminosities of $\log(L/L_\odot) = 5.7$ are lower limits from the M_v–W(O I λ7774) relationship (Arellano Ferro et al. 2003; Clark et al. 2005).

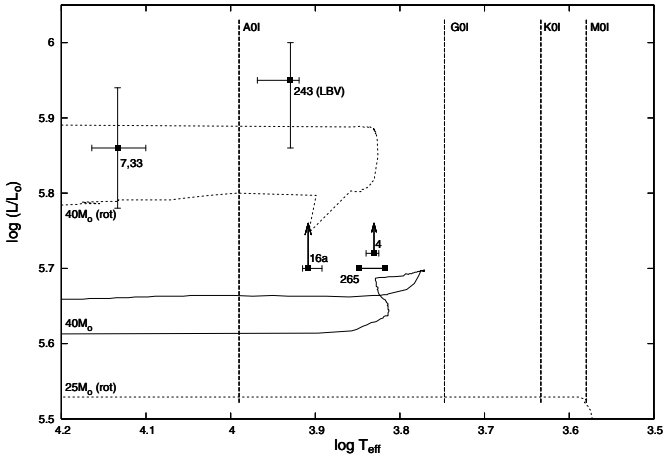

Fig. 5. Location of luminous hypergiants in Wd1 for a distance of 5 kpc compared to $z = 0.020$ (i.e. solar abundance) evolutionary tracks with and without rotation (Meynet & Maeder 2003). Lower limits for the luminosities of the YHGs W4, W16a and W265 are plotted. W4 is offset vertically by 0.02 dex and error bars are omitted for W265 to highlight the change in spectral type over the pulsational cycle.

non-coevality in Wd1 (Negueruela et al. 2010) and the location of two RSGs near the core of the cluster argue against the RSGs being descended from a separate population of older, lower-mass stars. Short-term spectroscopic variability and lack of contemporaneous photometry render the luminosities of individual RSGs uncertain, and further observations are required to place them firmly on the HR diagram. Nevertheless, the M1−5Ia spectral types derived from TiO band strengths appear robust (Clark et al. 2010a), and are clearly discrepant with respect to current theoretical predictions.

4.2.2. The Wd1 magnetar

The magnetar CXOU J164710.2-455216 (Muno et al. 2006, 2007) lies 1.′7 from the centre of Wd1, corresponding to 2.3(d/5 kpc) pc in projection. The negligible likelihood of the magnetar being a chance association and the presence of ∼O8V stars in Wd1 provide strong evidence for a massive progenitor (Muno et al. 2006), a result confirmed by our direct measurement of the mass of W13 which rules out a magnetar progenitor below ∼35 $M_\odot$ and strongly supports a progenitor mass in excess of ∼45 $M_\odot$ unless mass transfer within W13 is unexpectedly conservative. This is consistent with the expected initial masses of the most evolved WR stars in Wd1, and also progenitor masses derived for other magnetars: a 48^{+20}_{-8} $M_\odot$ progenitor mass is found for the magnetar SGR1806-20 based on its assumed membership of a massive cluster at G10.0-0.3 (Bibby et al. 2008), while an expanding HI shell around the magnetar 1E 1048.1-5937 is inferred to be a wind-blown bubble from a ∼30−40 $M_\odot$ progenitor (Gaensler et al. 2005). The progenitor of SGR1900+14 has a significantly lower mass (Clark et al. 2008; Davies et al. 2009), implying a number of formation pathways exist. However, the derived mass of SGR1806-20 is strongly influenced by the distance to the host cluster obtained from spectroscopic observations, and our results place the first *dynamical* constraints on a massive magnetar progenitor. Indeed, our results suggest that CXOU J164710.2-455216 may have the highest dynamically-constrained progenitor mass of *any* confirmed neutron star. The high-mass X-ray binary 4U1700-37 contains a O6.5Iaf$^+$ mass donor with mass 58 ± 11 $M_\odot$ but the nature of the 2.44 ± 0.27 $M_\odot$ compact object remains uncertain (Clark et al. 2002), while the ∼43 ± 10 $M_\odot$, highly-luminous B1Ia$^+$ hypergiant in the X-ray binary Wray 977/GX 302-2 may have evolved via quasi-conservative Case A transfer in a 3.5 day binary with initial masses 26 $M_\odot$ + 25 $M_\odot$ (Wellstein & Langer 1999; Kaper et al. 2006).

NTT/SofI K_s-band imaging rules out a current ≥1 $M_\odot$ companion to the magnetar (Muno et al. 2006), a result we confirm using deep VLT/NACO J-, H- and K_s-band imaging (Clark et al., in prep.). Nevertheless, given the high binary fraction amongst the WR population (Crowther et al. 2006) and the need for a low pre-supernova core mass to avoid direct (or fallback) black hole formation (e.g. Fryer et al. 2002) it would appear likely that the magnetar progenitor *was* part of a (now-disrupted) close binary system (Clark et al. 2008). Support for this hypothesis comes from population synthesis models, which can only form a neutron star from an isolated ∼60 $M_\odot$ progenitor within the ∼5 Myr age of Wd1 if mass loss rates from stellar winds are greatly enhanced (Belczynski & Taam 2008). In a close binary scenario, however, removal of the hydrogen-rich outer mantle via Case A mass transfer results in a reduced post-MS helium core, and ongoing Case B transfer during shell burning will leave a low mass (≤10 $M_\odot$) helium-burning WR (P05), permitting isolated neutron star formation within 5 Myr via a type Ib/c supernova if the kick velocity is sufficient to disrupt the system[10]. Neutron star formation may also occur for massive binaries with initial periods greater than a few weeks; such systems will not undergo Roche lobe overflow until core hydrogen burning is complete and therefore form higher-mass helium cores than Case A systems, but if Case B or early-Case C mass transfer can suppress hydrogen shell burning before core helium burning is complete then the consequent reduction in the mass of the iron core may limit black hole formation (Brown et al. 2001). Further results on the distribution of binaries on Wd1 from our VLT/FLAMES survey and follow-up observations will therefore allow strong constraints to be placed on the formation channels for such systems.

5. Conclusions and future work

We find lower mass limits for the components of the eclipsing binary W13 of 21.4 ± 2.6 $M_\odot$ and 32.8 ± 4.0 $M_\odot$, rising to $23.2^{+3.3}_{-3.0}$ $M_\odot$ and $35.4^{+5.0}_{-4.6}$ $M_\odot$ for our best-fit inclination 62^{+3}_{-4} degrees, with spectroscopy suggesting that the evolved emission-line object is likely an immediate evolutionary precursor to the WR phase. As conservative mass transfer would require the exchange of (at least) 5−10 $M_\odot$ without the accretor exceeding critical rotation, it appears likely that W13 evolved through non-conservative late-Case A/Case B mass transfer as the (initially) more massive star left the MS. Estimates of the initial WR mass from P05 and the presence of a ≥33 $M_\odot$ supergiant companion, which cannot have greatly increased in mass during highly non-conservative transfer, therefore suggest a MS mass for the emission-line object in excess of ∼40 $M_\odot$. This is consistent with previous estimates of the transitional supergiant masses in Wd1 obtained from the MS turnoff and spectroscopy of the WR and OB supergiant populations (Crowther et al. 2006; Clark et al. 2010a; Negueruela et al. 2010). Most importantly, this result places the first dynamical constraint on the mass of a magnetar progenitor, and highlights a discrepancy between the presence of

[10] In this scenario, ∼90% of the MS mass of the primary is lost prior to SN, with the secondary ultimately forming an isolated black hole with M_{BH} ∼ 8 $M_\odot$ (Belczynski & Taam 2008).

RSGs in Wd1 and the predictions of evolutionary models, which suggest that the most luminous RSGs should evolve from significantly lower masses.

A first study of the binary fraction amongst lower-luminosity late-O II−III stars in Wd1 will be presented in a subsequent paper in this series, but many binary systems are already available for follow-up study. These include short-period spectroscopic binaries (W43a, W3003; Paper I), eclipsing binaries within the WR, OB supergiant and main sequence populations (Bonanos 2007), and X-ray and radio-selected colliding-wind binaries (Clark et al. 2008; Dougherty et al. 2010). Consideration of these data will allow further dynamical constraints to be placed on the progenitor masses of the evolved stars within Wd1 as well as the general mass luminosity relation for stars in the upper reaches of the HR diagram and the post-MS pathways they follow. Moreover, they will yield the first characterisation of the binary properties of a homogeneous population of massive stars, of critical importance for studies of both star and cluster formation and numerous high-energy phenomena such as supernovae, Gamma-ray bursters and the formation of high mass X-ray binaries.

Acknowledgements. We thank Alceste Bonanos for making photometry of Westerlund 1 publicly available, Rainer Wichmann for the nightfall code, Paul Crowther for comments on a draft of this manuscript, and an anonymous referee for a detailed and constructive report. J.S.C. gratefully acknowledges the support of an RCUK fellowship. I.N. has been funded by grants AYA2008-06166-C03-03 and Consolider-GTC CSD-2006-00070 from the Spanish Ministerio de Ciencia e Innovación (MICINN).

References

Andersen, J. 1975, A&A, 44, 355
Arellano Ferro, A., Giridhar, S., & Rojo Arellano, E. 2003, Rev. Mex. Astron. Astrofis., 39, 3
Belczynski, K., & Taam, R. E. 2008, ApJ, 685, 400
Bibby, J. L., Crowther, P. A., Furness, J. P., & Clark, J. S. 2008, MNRAS, 385, 544
Bonanos, A. Z. 2007, AJ, 133, 2696
Brown, G. E., Heger, A., Langer, N., et al. 2001, NewA, 6, 457
Clark, J. S., Goodwin, S. P., Crowther, P. A., et al. 2002, A&A, 392, 909
Clark, J. S., Negueruela, I., Crowther, P. A., & Goodwin, S. 2005, A&A, 434, 949
Clark, J. S., Muno, M. P., Negueruela, I., et al. 2008, A&A, 477, 147
Clark, J. S., Ritchie, B. W., & Negueruela, I. 2010a, A&A, 514, A87
Clark, J. S., Najarro, P., Negueruela, I., Howarth, I. D., & Ritchie, B. W. 2010b, A&A, in prep.
Crowther, P. A., & Smith, L. J. 1997, A&A, 320, 500
Crowther, P. A., Hadfield, L. J., Clark, J. S., Negueruela, I., & Vacca, W. D. 2006, MNRAS, 372, 1407
Davies, B., Figer, D. F., Kudritzki, R.-P., et al. 2009, ApJ, 707, 844
Dougherty, S. M., Clark, J. S., Negueruela, I., Johnson, T., & Chapman, J. M. 2010, A&A, 511, A58
Drout, M. R., Massey, P., Meynet, G., Tokarz, S., & Caldwell, N. 2009, ApJ, 703, 441
Efron, B., & Tibshirani, R. J. 1994, An Introduction to the Bootstrap (Boca Raton, FL: CRC Press)
Fryer, C. L., Heger, A., Langer, N., & Wellstein, S. 2002, ApJ, 578, 335
Fullerton, A. W., Massa, D. L., & Prinja, R. K. 2006, ApJ, 637, 1025
Gaensler, B. M., McClure-Griffiths, N. M., Oey, M. S., et al. 2005, ApJ, 620, 95
Gies, D. R. 2003, in A Massive Star Odyssey: From Main Sequence to Supernova, ed. K. A. van der Hucht, A. Herrero, & C. Esteban, IAU Symp., 212, 91
Humphreys, R. M., Davidson, K., & Smith, N. 2002, ApJ, 124, 1026
Humphreys, R. M., Jones, T. J., Polomski, E., et al. 2006, AJ, 131, 2105
Kaper, L., van der Meer, A., & Najarro, F. 2006, A&A, 457, 595
Langer, N. 1998, A&A, 329, 551
Langer, N., Cantiello, M., Yoon, S.-C., et al. 2008, in Massive Stars as Cosmic Engines, ed. F. Bresolin, P. A. Crowther, & J. Puls, IAU Symp., 250, 167
Linder, N., Rauw, G., Manfroid, J., et al. 2009, 495, 231
Massey, P., & Conti, P. S. 1977, ApJ, 218, 431
Meynet, G., & Maeder, A. 2000, A&A, 361, 101
Meynet, G., & Maeder, A. 2003, A&A, 404, 975
Mokiem, M. R., de Koter, A., Vink, J. S., et al. 2007, A&A, 473, 603
Muno, M. P., Clark, J. S., Crowther, P. A., et al. 2006, ApJ, 636, L41
Muno, M. P., Gaensler, B. M., Clark, J. S., et al. 2007, MNRAS, 378, 44
Negueruela, I., & Clark, J. S. 2005, A&A, 436, 541
Negueruela, I., Clark, J. S., & Ritchie, B. W. 2010, A&A, 516, A78
Packet, W. 1981, A&A, 102, 17
Pasquani, L., Avila, G., Blecha, A., et al. 2002, The Messenger, 110, 1
Petrovic, J., Langer, N., & van der Hucht, K. A. 2005, A&A, 435, 1013 (P05)
Press, W. H., & Rybicki, G. B. 1989, ApJ, 338, 277
Rauw, G., Nazé, Y., Carrier, F., et al. 2001, A&A, 368, 212
Rauw, G., Crowther, P. A., Eenens, P. R. J., Manfroid, J., & Vreux, J.-M. 2002, A&A, 392, 563
Ritchie, B. W., Clark, J. S., Negueruela, I., & Crowther, P. A. 2009a, A&A, 507, 1585 (Paper I)
Ritchie, B. W., Clark, J. S., Negueruela, I., & Najarro, F. 2009b, A&A, 507, 1597
Simon, K. P., & Sturm, E. 1994, A&A, 281, 286
Southworth, J., & Clausen, J. V. 2007, A&A, 461, 1077
van Helden, R. 1972, A&A, 19, 388
Walborn, N. R., Stahl, O., Gamen, R. C., et al. 2008, ApJ, 683, 33
Wellstein, S., & Langer, N. 1999, A&A, 350, 148
Westerlund, B. E. 1961, PASP, 73, 51